A Blind Watermarking Using Orthogonal Finite Ridgelet Transform and Fuzzy C-Means

Hai-Yan Yu Jiu-Lun Fan
Dept. of Information and Control, Xi'an Institute of Post and Telecommunications, Xi'an, Shaanxi, China
Email: yuhaiyan2010@yahoo.com.cn, jiulunf@xupt.edu.cn

***Abstract*—Based on energy distribution analysis of orthogonal FRIT coefficients, a novel digital image watermark embedding and blind detecting algorithm in ridgelet domain is proposed in this paper. Since the ridgelet transform has directional sensitivity and anisotropy, the image is first partitioned into small pieces and the orthogonal FRIT is applied for each piece to obtain a sparse representation of the image, especially for straight edge singularity. Through analyzing texture distribution in ridgelet coefficients of each piece, these image pieces are classified into frat regions and texture regions by Fuzzy C-Mean (FCM) clustering algorithm. The texture regions used for watermark embedding also classified into two regions, strong texture regions and week texture regions for different embedding strengths based on the features of luminance masking and texture masking. And the watermarks can be blindly detected without the original image and watermark information. Experimental results show that the proposed watermarking scheme can achieve a better tradeoff between the robustness and the transparency.**

***Index Terms*—image processing, blind watermarking, ridgelet transform, Fuzzy C-Mean**

I. INTRODUCTION

Digital watermarking is a technique to protect the image against unauthorized use. The watermarking should not alter visibly the image and be robust to alterations which may be caused by various image processing techniques. The image watermarking algorithms can be classified into two categories: spatial domain techniques and frequency domain techniques. The former ones directly modify the intensities or color values of some selected pixels while the latter ones modify the values of some transformed coefficients. In the recent past, watermarking methods operating in the discrete Fourier transform, in the discrete cosine transform domain (DCT) [1] and in the discrete wavelet transform domain (DWT) [2], have been proposed.

Candes and Donoho pioneered a new system of representations named ridgelets which can deal effectively with line singularities in two dimensions [3] and overcome the weakness of wavelets in higher dimensions. Do and Vetterli proposed finite ridgelet transform(FRIT) which is a discrete means of realizing the ridgelet transform for representation of linear sigularitities [4]. After the Finite Radon Transform (FRAT) mapping linear singularities in image domain to point singularities in FRAT domain, a collection of orthogonal transforms are applied to FRAT coefficients column wisely to accomplish the FRIT. The resulting transform is invertible, non-redundant and leads to a family of directional orthogonal bases for digital images. However, the intrinsic "wrap around" effect of FRAT restricts heavily the representation of image texture and direction energy for FRIT [5], [6]. Do and Vetterli proposed an orthonormal version of the ridgelet transform by introducing an ordering of the FRAT coefficients to overcome the periodization effect of a finite transform to some extent [5]. In this paper a novel blind watermarking algorithm operating in ridgelet domain is proposed combined with the statistical study of energy distribution in the FRIT domain and the characteristics of the Human Visual System (HVS).

Since edges in images are typically curves, in order to obtain an effective image representation through the ridgelet transform, the image is partitioned into pieces of side-length such that an edge appears as a straight line. With human visual masking of HVS, the weaker the texture of the image regions, the more sensitive the noise in these regions. So the image pieces undergo twice classifications for the determinations of watermark embedding locations and strengths. Firstly, they can be classified into two groups: frat pieces and texture pieces, where the latter ones are used for the watermark embedding. Secondly, the texture pieces are also classified into strong texture pieces and weak texture pieces for different watermark embedding strengths to provide a better tradeoff between the robustness and transparency based on luminance and texture masking characteristics. Xie [7] proposed a method of the piece classification for watermark embedding in ridgelet domain. But it seems to select incomplete texture pieces. In this paper Fuzzy C-Mean (FCM) algorithm [8] is used for the classification based on the study of energy distributions in FRIT domain and HVS. For better description of the image texture degree in ridgelet domain, two features are considered into FCM for the piece classifications. The fist feature is the total variation of each direction in the FRIT domain within a piece. The second feature is the total energy of the energy dispersion directions to make up for the "wrap around" effect for FRIT on representation of the image texture in those directions. Meanwhile the two features should be nonlinearly processed because of the limitation of FCM algorithm based on the approximate logarithms characteristic of human visual system before classifying

doi:10.4304/jsw.5.4.429-436

the pieces. Within the texture pieces, the middle ridgelet subband coefficients of the most significant directions are selected to embed watermark signal with different strengths. Experiments show that our method can achieve better tradeoff between the robustness and transparency.

II. RIDGELET TRANSFORM

A. Continuous Ridgelet Transform

We start by briefly reviewing the continuous ridgelet transform and draw its connection with the continuous wavelet transform. Given an integrable bivariate function $f(X)$, the continuous ridgelet transform in R^2 can be defined by

$$RI_f(a,b,\theta) = \int \psi_{a,b,\theta}(X) f(X) dX . \quad (1)$$

For each $a > 0$, $b \in R$ and $\theta \in [0, 2\pi)$, the bivariate ridgelet $\psi_{a,b,\theta}(X) : R^2 \to R^2$ is defined by

$$\psi_{a,b,\theta}(X) = a^{-1/2} \psi((x_1 \cos\theta + x_2 \sin\theta - b)/a) . \quad (2)$$

where a is a scale parameter, b a shift parameter, and $X = (x_1, x_2)^T$. Hence, a ridgelet is constant along the line $x_1 \cos\theta + x_2 \sin\theta - b = const$ and has the shape of the wavelet $\psi_{a,b}(x) = a^{-1/2}\psi((t-b)/a)$ in the perpendicular direction. Transverse to these ridges it is a wavelet. And the exact reconstruction formula is

$$f(X) = \int_0^{2\pi} \int_{-\infty}^{\infty} \int_0^{\infty} RI_f(a,b,\theta) \psi_{a,b,\theta}(X) \frac{da}{a^3} db \frac{d\theta}{4\pi} . \quad (3)$$

A basic tool for calculating ridgelet coefficients is to view ridgelet analysis as a form of wavelet analysis in Radon domain. The Radon transform of an object f is the collection of line integrals indexed by $(\theta, t) \in [0, 2\pi) \times R$, and is given by

$$RA_f(\theta, t) = \int_{R^2} f(X) \delta(x_1 \cos\theta + x_2 \sin\theta - t) dX . \quad (4)$$

Then the ridgelet transform is precisely the application of a 1-D wavelet transform to the slices of the Radon transform,

$$RI_f(a,b,\theta) = \int RA_f(\theta,t) a^{-1/2} \psi((t-b)/a) dt . \quad (5)$$

Finally the original function can be reconstructed by applying 1-D inverse wavelet transform to each slices and inverse Radon transform.

B. Orthogonal Finite Ridgelet Transform

Finite Ridgelet Transform (FRIT) is a discrete means of realizing the ridgelet transform on a 2-D digital image with finite size, which is realized by applying 1-D wavelet transform on the Finite Radon Transform(FRAT) [9]. Denote $Z_p = \{0, 1, 2, ..., p-1\}$, where p is a prime number. Discrete lines on Z_p^2 is defined as:

$$L_{k,l} = \begin{cases} \{(i,j) : j = (ki + l) \bmod p, i \in Z_p\}, & k \in Z_p, l \in Z_p \\ \{(l,j) : j \in Z_p\}, & k = p, l \in Z_p \end{cases} . \quad (6)$$

The FRAT of a real function I on Z_p^2 is defined as summations of image pixels over the discrete lines

$$r_k[l] = FRAT_I(k,l) = \frac{1}{\sqrt{p}} \sum_{(i,j) \in L_{k,l}} f(i,j) . \quad (7)$$

It has been demonstrated that FRAT is invertible, thus providing a representation for a generic image. With the invertible FRAT, FRIT is obtained by taking the discrete wavelet transform on each vector by applying (5). Note that the FRAT is redundant and not orthogonal. An orthonormal FRIT is proposed in [4] to remove this redundancy by taking the 1-D DWT on the projections of the FRAT in a special way. Assume $\{w_m^{(k)} : m \in Z_p\}$, $0 \le k \le p$ to be $p+1$ orthogonal bases in $l^2(Z_p)$ that satisfy the condition Z, then $\{p_{k,m} : k = 0, 1, ..., p; m = 1, 2, ..., p-1\} \cup \{P_0\}$ is an orthogonal basis in $l^2(Z_p^2)$. The expansion of the original image f on these bases gives out the FRIT coefficients, and the overall transform is named as orthogonal finite ridgelet transform. That is to say, after 1-D orthogonal transforms satisfying condition Z applied to FRAT columns, the $p-1$ detail coefficients of each column together with the common scaling coefficient of all $p+1$ columns constitute the FRIT coefficients of f. Then, after the columnwise inverse orthogonal transform and IFRAT, one obtains the reconstruction image. Furthermore, due to the "wrap around" effect of the FRAT, its projections could have strong periodicity components, so for some projections one could use a Fourier-type transform like DCT [4]. A fixed FRIT scheme proposed by Do and Vetterli [5] which applies DWT into 16 directions with less "wrap around" effect and DCT to other directions in FRAT domain, is used to realizing the ridgelet transform of an image in this paper and denoted as FRIT for convenience in the following sections.

III. THE PROPOSED WATERMARKING ALGORITHM

With human visual masking of HVS, the noise in flat regions of image is more sensitive than that in texture regions. The detection threshold values's height of human to the weak signal superposed on the strong background is determined by the luminance, texture complexity and the frequency of the background, which indicates that the local regions of different local properties in an image can superpose watermarks with different strengths on the premise of the imperceptibility [10]. In this paper, a watermark algorithm is proposed based on the local properties in the ridgelet domain, which is illustrated as Fig.1.

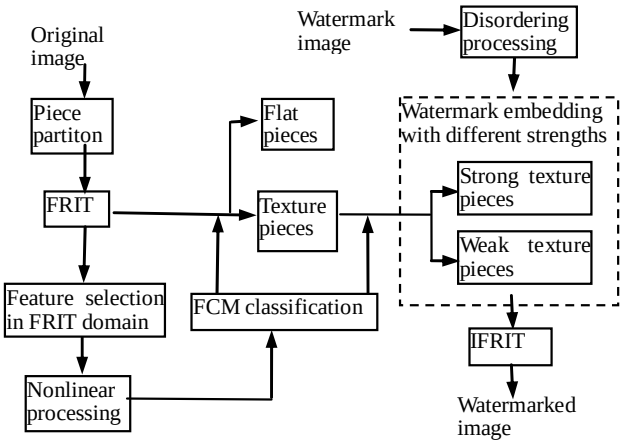

Figure 1. The diagram of the proposed watermarking system.

The original image is first partitioned into pieces whose size is such that a curved edge appears to be straight. Then the FRIT is performed on each piece. Based on the statistic study of energy distribution in FRIT domain, the image pieces are firstly classified into two groups, flat pieces and texture pieces, by FCM cluster algorithm with the distribution of the directional energy as feature vectors. And the vectors undergo a nonlinear processing based on the approximate logarithms characteristic of human visual system before classification. The texture pieces are selected for watermark embedding, while the flat pieces disagree with the watermark embedment because of its high selectivity to the noise. Secondly the texture pieces are also classified into two groups, weak texture pieces and strong texture pieces, based on the representation characteristics of ridgelet coefficients for local image texture and edges. Then watermark is embedded into these texture pieces with different embedment strengthes. Finally, the inverse FRIT is performed, thus obtaining the watermarked image.

A. Twice piece classifications with FCM algorithm

1) Feature matrix determination in FRIT domain: Given an original image X that is split into non-overlapped pieces of denoted X_h, $h=1,2,...,H$. For each piece, the digital ridgelet transform is applied to get ridgelet coefficients $FRIT_{X^h} = \{FRIT_{X^h}[k,l],\ (k,l) \in P_{ij}\}$. Then the ridgelet coefficient energy of the direction k is obtained by $E_{k_h} = \sum_{l=0}^{p-1}(FRIT_{X_h}[k,l])^2$. The energy of all the directions can be represented as a set $E = \{E_0, E_1, ..., E_p\}$. Then two distribution features of the directional energy in the FRIT domain are considered into the representation of the texture activity degree. The fist feature is the total variation of each direction in the FRIT domain within a piece [11].

$$TV = \sum_{s=1}^{p} |E_s - E_{s-1}|. \qquad (8)$$

The second feature is the total energy of the energy dispersion directions to make up for the "wrap around" effect for the FRIT on representation of the image texture in those directions. The "wrap around" effect caused by the module operation in (6) disperses the energy of the natural straight lines in the FRAT domain, which is presented as periodic oscillation of the FRAT coefficients in some projection directions and reflects the energy dispersion situation of the natural straight lines in other projection directions. The distributions of the oscillating coefficients are influenced by complex factors, such as the locations and lengths of the straight lines, the overlapping degree of the different straight lines, and the statistical characteristics of an image, which is also a main problem for FRAT to be solved [5], [6]. Based on the statistical study on the directional energy distributions in the FRIT domain, for almost each texture image, energy tends to distribute mainly in the vertical and horizontal directions, the second in $\pi/4$ and $\pi 3/4$ directions, and the third in the other directions, because of the module operation. Let the horizontal, vertical, $\pi/4$ and $\pi 3/4$ directions be the main energy directions, which are represented by E_h, E_v $E_{\pi/4}$ and $E_{\pi 3/4}$ respectively. Let the other directions be the energy dispersion directions, of which the total energy is

$$EF = (\sum_{i=1}^{p+1} E_i) - E_h - E_v - E_{\pi/4} - E_{3\pi/4}. \qquad (9)$$

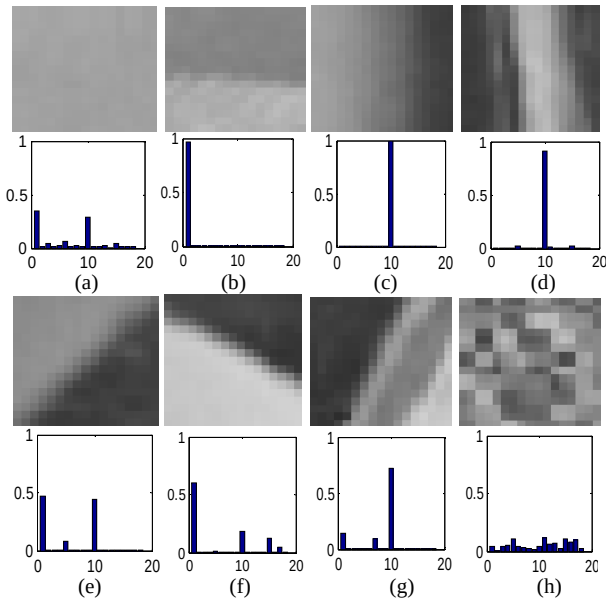

Figure 2. (a)-(h): Eight typical texture image pieces (up) and energy ratios of the 18 directions corresponding to the eight pieces (down).

Let $NF = EF / \sum_{i=1}^{p+1} E_i$ denote the energy ratio of the energy dispersion directions. Fig. 2 shows the energy ratios of the 18 projection directions of eight 17×17 typical pieces with different texture distributions. The energy ratios of the horizontal, vertical $\pi/4$ and $\pi 3/4$ directions are the 1st, 10th, 5th and 15th columns,

respectively. The more active the texture in the energy dispersion directions, the bigger the energy ratio of those directions, as shown in Tab. 1. In order to strengthen representation of the degree of the texture activity for the dispersion energy directions, the total energy of those directions EF is used as an evaluation index of the texture activity degree.

TABLE I.
THE DIRECTION ENERGY DISTTIBUTIONS IN FRIT DOMAIN OF THE SELECTED TYPICAL TEXTURE IMAGE PIECES

Distribution feature	(a)	(b)	(c)	(d)	(e)	(f)	(g)	(h)
TV (*10^5)	0.002	0.182	1.352	1.174	0.950	2.224	2.194	0.133
EF (*10^5)	0.009	0.065	0.013	0.470	0.064	2.289	2.514	2.365
NF	0.298	0.022	0.001	0.048	0.006	0.086	0.126	0.696

Let the distribution features $TV(h)$ and $EF(h)$ corresponding to image piece X_h constitute an eigenvector $TZ(h)$ for FCM algorithm by $TZ(h) = [TV(h), EF(h)]$. Then the eigenvector are considered into the classifications of image pieces with FCM algorithm considering the feature of luminance masking and texture masking. Firstly the image pieces are classified into frat pieces and texture pieces, of which the later ones are selected for watermark embedding. Since the more active the texture in an image piece, the stronger the watermark embedding strength can be. Secondly, the selected texture pieces are also classified into weak pieces and strong pieces for watermark embedding with different strength.

2) Nonlinear processing of the feature matrix and twice classification with FCM: Given a feature vector space $X = \{X_1, X_2, ..., X_M\}$, where M is the number of the elements. The feature vector space is partitioned into C ($1 < C < M$) fuzzy subclasses. The classification matrix $U = \{\mu_{ij}\}$ is a fuzzy matrix, where μ_{ij} is the degree of the membership of $U = \{\mu_{ij}\}$ in the j th cluster and $\mu_{ij} \in [0,1]$, $\sum_{i=1}^{C} \mu_{ij} = 1$, where $1 \le i \le M, 1 \le j \le C$. The cluster criteria is to minimize the objective function

$$J_0^*(U,V) = \sum_{i=1}^{n}\sum_{j=1}^{c}(\mu_{ij})^m (d_{ij})^2, 1 \le m < \infty . \quad (10)$$

where $V_j = (\sum_{j=1}^{C}(\mu_{ij})^m X_j) / \sum_{j=1}^{C}(\mu_{ij})^m$ is the center of cluster j, $(d_{ij})^2 = \|X_i - V_j\|^2 = \sum_{l=1}^{s}(X_{il} - V_{jl})^2$ is the distance between X_i and the center of cluster V_j, and m is the weighted exponent on each fuzzy membership [8].

The eigenvectors $TZ(h) = [TV(h), EF(h)]$ of all the pieces X_h with $h = 1, 2, \cdots, H$ of an image constitute a feature matrix **TZ**, namely the feature vector space. Let number of the fuzzy subclasses $C = 2$, the weighted exponent $m = 2$. Then the optimal matrix $U = \{\mu_{ij}\}$ and the center of clusters $V = \{V_1, V_2\}$ would be calculated by searching for minimum $J_0^*(U,V)$ to obtain optimal fuzzy clustering. For the first classification, two clusters ω_1 and ω_2 are obtained, of which the cluster whose center is bigger value represents the texture pieces with higher luminance and texture complexity and is suitable for watermark embedding. Let this cluster be ω_2 and represented by the set $Y = \{Y_b \in \omega_2, b = 1, 2, ..., B\}$. For the second classification of the texture pieces ω_2, two clusters ω_{21} and ω_{22} respectively representing the weak and strong texture pieces are obtained for watermark embedding with different strength.

As many c-means algorithms, FCM denotes class only by class center, which can only fit to sphere-like type of cluster. Statistical data show that the elements of the feature matrix **TZ** are dispersively distributed, which make FCM unable to deal with the situation very well. In this paper the feature matrix **TZ** will be processed beforehand to enhance the separability of the sample data. As is known, there is typical link of an approximate logarithm mapping in the process from receiving signal for human eye to forming an image in the brain. So feature TV and EF are adjusted with a logarithm processing.

$$TV'(h) = \log(TV(h)), EF'(h) = \log(EF(h)) . \quad (11)$$

Then the eigenvector of the corresponding image piece X_h is modified by $TZ'(h) = [TV'(h), EF'(h)]$ and constitutes a feature matrix **TZ'**.

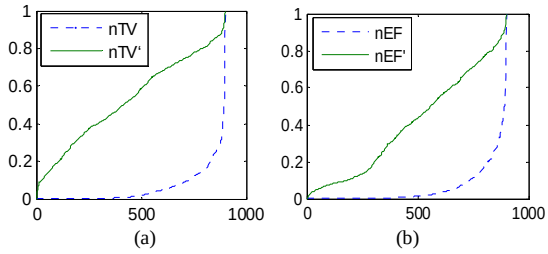

Figure 3. (a) The distribution maps of the normalized feature vectors *TV* and *TV'* in increasing order; (b) The distribution maps of the normalized feature vectors *EF* and *EF'* in increasing order.

Fig.3 (a), (b) show the comparison of distribution map of pre and post nonlinear processing of the feature matrix of the 510×510 Lena image shown in Fig.4(c), which is partitioned into pieces with $N \times N (N = 17)$. The feature value is in an increasing order within the $H = 900$ pieces. And nTV, nTV', nEF and nEF' are corresponding to the normalized feature vectors TV, TV', EF and EF'.

Fig.4 (a) shows the classification result with the feature matrix **TZ** without nonlinear processing, where the red and blue dots represent the sets of the flat pieces ω_1 and

texture pieces ω_2, respectively. The black star points represent the centers of the two clusters. Fig. 4 (b) shows the classification result with the feature matrix $\mathbf{TZ}'$. Fig. 4(c) and (d) show the classification results of the pieces pre and post nonlinear processing of feature matrix, where the black pieces representing the texture image pieces for the next classification and the watermark embedding. Obviously, the nonlinear processing makes the FCM obtain better classification results. Theoretically from human visual characteristics, the nonlinear processing can inhibit the high energy and extend the low energy, which can make the classification results of image pieces with FCM agree with the human visual characteristics better. Fig. 4 (e) and (f) show the second classification results of the texture pieces corresponding to first classification results, where the black and the white pieces representing the weak pieces ω_{21} and strong texture pieces ω_{22}, respectively. It is clear that our method can also get most of strong texture pieces with feature vectors being nonlinear processing, only with a small part of texture pieces being wrongly classified into weak pieces.

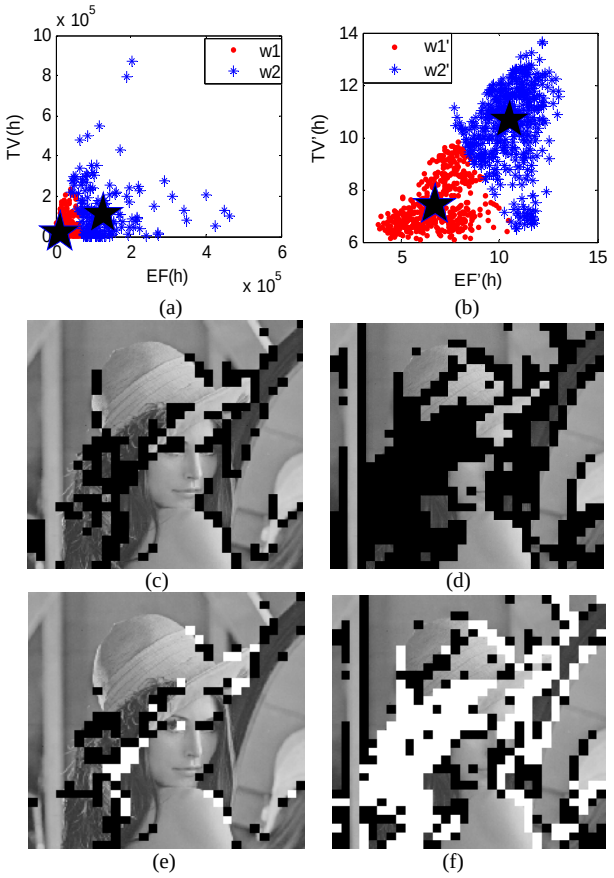

Figure 4. (a)-(b) The distribution maps of the feature matix *TZ* and *TZ'* of the first classification; (c)-(d) The first classification results of the image pieces of the pre and post nonlinear processing of the feature matix; (e)-(f) The second classification results of the selected texture pieces of the pre and post nonlinear processing of the feature matix.

B. Watermark embedding

A dual-value watermark logo is scanned from left to right and from top to down to produce a watermark sequence $W=[w_1,w_2,...w_M]$, with length of M. $\{w_l\}$ is disordered to get a new sequence $\tilde{W}$ by $\tilde{w}_l = w_l \oplus r_l$, where '$\oplus$' is a XOR operation and $\{r_l\}$ with length of M is a pseudo-random sequence generated by a secret Key.

After the first piece classification of the original carrier image with FCM, the pieces $\{Y_b \in \omega_2, b=1,2,...,B\}$ for watermark embedding are selected. The direction l_k within the piece Y_b which has the higher energy than others and thus higher robustness towards signal processing can be used for watermark embedment. It is obtained by $l_k = \max(\sum_{l=0}^{p-1}(FRIT_{Y_i}[k,l])^2)$. With regard to imperceptibility, the human visual system is less sensitive to high frequencies. But with regard to robustness, processing such as noise attack always modifies high frequencies and preserves low frequencies [12]. As a compromise, this paper chooses the middle ridgelet subband in the direction l_k for watermark embedding as a tradeoff between imperceptible and robustness. Let the number of these coefficients in the direction l_k be n, where $n=\lceil M/B \rceil$. The vectors composed of the ridgelet coefficients of the direction with the biggest energy l_k of the selected pieces $Y_h \in Y$ are represented as $V_l=[I_{1,l}, I_{2,l},..., I_{n,l}]$ and constitute an embedding matrix $I=[V_1,V_2,...,V_B]=\{I_{ij}\}_{n\times B}$, which will be embedded into watermark sequence $\{\tilde{w}_l\}$ row by row.

On the assumption that $Z_{ij} = I_{ij} \bmod S_{ij}$, S_{ij} is a given quantized value applied to adjust the depth of watermark embedded. As it mentioned above, the texture pieces selected for watermark embedding are classified into two groups: weak texture pieces ω_{21} and strong texture pieces ω_{22}. Considering to a better tradeoff between imperceptibility and robustness in the same image, the strength S_{ij} should be different corresponding to the different texture activity of the texture image piece. It is determined by

$$\begin{cases} S_{ij} = S1, & I_{ij} \in \omega_{21} \\ S_{ij} = S2, & I_{ij} \in \omega_{22} \end{cases}. \qquad (12)$$

where $S1 < S2$, which are determined based on the visual quality of the watermarked image by experiments in this paper. Then the disordered watermark sequence $\tilde{W}$ is embedded by the following method.

When $\{\tilde{w}_l\}=0$,

$$I'_{ij} = \begin{cases} I_{ij} + S_{ij}/4 - Z_{ij}, & Z_{ij} \in [0, S_{ij}*3/4) \\ I_{ij} + S_{ij}*5/4 - Z_{ij}, & Z_{ij} \in [S_{ij}*3/4, S_{ij}) \end{cases}. \qquad (13)$$

When $\{\tilde{w}_l\}=1$,

$$I'_{ij}=\begin{cases} I_{ij}-S_{ij}/4-Z_{ij}, & Z_{ij}\in[0,S_{ij}/4) \\ I_{ij}+S_{ij}*3/4-Z_{ij}, & Z_{ij}\in[S_{ij}/4,S_{ij}) \end{cases}. \quad (14)$$

Finally, the ridgelet coefficients of each piece are applied inverse-FRIT to get watermarked image.

C. Watermark extraction

The watermark blind extracting is performed by applying dual operations with respect to the ones performed for watermark embedding without the original image. Specifically, given a possibly corrupted image, the same piece portioning and FRIT transform is performed for each piece. The category of each piece is obtained by the same method in the watermark embedding process. The middle subband ridgelet coefficients of the directions with the highest energy within the selected pieces are selected and collected into the embedded matrix: $I'=\{I'_{ij}\}_{n\times B}$. Then watermark sequence can be obtained by:

$$\tilde{w}'_l=\begin{cases} 0 & Z'_{ij}\in[0,S_{ij}/2) \\ 1 & Z'_{ij}\in[S_{ij}/2,S_{ij}) \end{cases}. \quad (15)$$

where $Z'_l=I'_{ij} \bmod S_{ij}$ and S_{ij} is determined according to (12). The watermark sequence W' is recovered by $w'_l=\tilde{w}'_l\oplus r_l$ based on the secret *Key* and reconstructs the watermark logo in the scanning order.

D. Performance analysis

We can take the measurement of the robustness of watermark algorithm by calculating the normalized autocorrelation function *NC*, which is defined as:

$$NC=\frac{\sum_l w_l w'_l}{\sum_l w_l^2}. \quad (16)$$

Meanwhile, the visual quality of watermarked and attacked images is measured using the peak signal to noise ratio (*PSNR*), which is defined as:

$$PSNR(dB)=10\log_{10}[\frac{\max_{\forall(m,n)} f^2(i,j)}{MSE}]. \quad (17)$$

where *MSE* is the mean square error:

$$MSE=\frac{\sum_{\forall(m,n)}(f_w(i,j)-f(i,j))^2}{mn}. \quad (18)$$

where m, n are the dimensions of the input image and f, f_w are the original and the watermarked images.

However, *PSNR* declines from the perceived subjective quality because the HVS does not correlate well with the square of the error. For this reason, the weighted peak signal to noise ratio (*WPSNR*) that takes into account the local texture masking is also used as follows [13]:

$$WPSNR(dB)=10\log_{10}[\frac{\max_{\forall(m,n)} f^2(i,j)}{MSE*NVF}]. \quad (19)$$

where $NVF(i,j)=1/(1+\theta\sigma_x^2(i,j))$ is a texture masking function using a Gaussian model to estimate how much texture exists in any area of an image. $\sigma_x^2(i,j)$ denotes the local variance of the image in a window centered on the pixel with coordinates (i,j) and is given as

$$\sigma_x^2(i,j)=\frac{1}{(2L+1)^2}\sum_{k=-L}^{L}\sum_{k=-L}^{L}(x(i+k,j+l)-\bar{x}(i,j))^2. \quad (20)$$

$$\bar{x}(i,j)=\frac{1}{(2L+1)^2}\sum_{k=-L}^{L}\sum_{k=-L}^{L}x(i+k,j+l). \quad (21)$$

θ is a tuning parameter corresponding to the particular image and is given as $\theta=D/\sigma_{x\max}^2$, where $\sigma_{x\max}^2$ is the maximum local variance for a given image and D is an experimental value, range from 50 to 100.

IV. Experimental Results and Analysis

The proposed watermarking algorithm is tested on two typical 510×510 images "Lena" and "Baboon" with different textural features, as shown in Fig. 5 (a) and (b), which is partitioned into pieces with $p\times p(p=17)$, thus obtaining $H=900$ pieces. A 30×27 binary image shown in Fig. 5 (c) is used as the watermark information which will be embedded into the carrier images. The performance measures are the invisibility of the inserted watermark and the robustness of the method against various types of attacks such as JPEG compression, median filtering, Gaussian noise and geometrical operations etc.

(a) (b) (c)

Figure 5. (a) Original carrier image Lena; (b) Original carrier image Baboon; (c) Watermark logo.

Firstly, to prove our good classification result of texture pieces, we compare with Xie's method [7]. Fig. 6(b) show the classification results of the Baboon image with Xie's method which obtain incomplete pieces with strong texture and edge features, compared with the classification result with our method. Fig. 6(a) shows the second classification results of the texture pieces. Obviously it get mostly strong texture image pieces for the Baboon image, where 338 strong texture pieces selected from the 538 texture pieces are suitable for watermark embedding with stronger strength, while the 200 weak texture pieces should be embedded watermark with low strength. The same goes for the Lena image.

The twice classification results of the Lena image have been shown in Fig. 4(d) and (f). 451 selected texture pieces are classified into 246 strong texture and 205 weak texture pieces for watermarking with different strength.

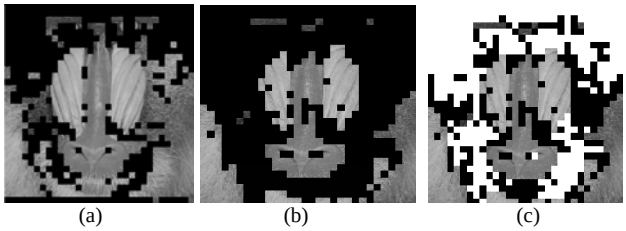

(a) (b) (c)

Figure 7. Baboon: (a) classification result with Xie's method; (b) the first classification result for frat pieces and texture pieces with our method; (c) the second classification result for weak texture pieces and strong texture pieces with our method.

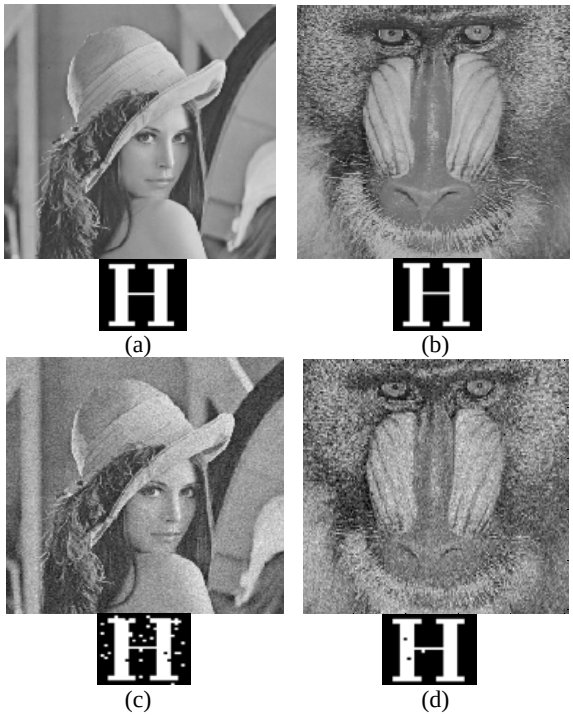

(a) (b) (c) (d)

Figure 6. (a) the watermarked image "Lena" with *PSNR*= 43.4 and *WPSNR*= 46.1 (up) and the extracted watermark logo with *NC*=1 (down); (b) the watermarked image "Baboon" with *PSNR*= 34.6 and *WPSNR*= 43.6 (up) and the extracted watermark logo with *NC*=1 (down); (c) the watermarked image "Lena" joined with Gaussian white noise of the mean value 0 and the variance 0.002, where *PSNR*= 26.3 and *WPSNR*= 28.9 (up) and the extracted watermark logo with *NC*=0.93 (down); (b) the watermarked image "Baboon" joined with Gaussian white noise of the mean value 0 and the variance 0.005, where *PSNR*= 21.5 and WPSNR= 29.2 (up) and the extracted watermark logo with *NC*=0.99 (down).

Fig. 7(a) shows the watermarked image of Lena with *PSNR*=43.4 and *WPSNR*= 46.1 and the extracted watermark logo with *NC*=1, where the watermark embedding strengths *S*1=80, *S*2=110. It is clearly see that the imperceptibility of the embedded watermarks is well guaranteed. Fig. 7(c) show the watermarked image joined with Gaussian noise of the mean value 0 and the variance 0.002 and the extracted watermark logo with *NC*= 0.93. It is clear that only few noisy dots found in the decoded watermark and the logo is still to be recognized by human eye.

Fig. 7(b) shows the watermarked image of Baboon indistinguishable from the original image with the watermark embedding strength *S*1=200, *S*2=250, which are much lager than that for Lena image. The *PSNR* is 34.6, which is below the generally acceptable threshold range [35~40 dB]. We still can not find perceptible distortion. This is because the human eye is less sensitive to the textured areas than smooth areas. Therefore, for different images, one may get a misleading result without considering the effect of HVS. However, *WPSNR* takes account into the effect of image texture on human eye, which can more precisely reflect the difference, just as the *WPSNR*=43.6 of the same watermarked Baboon image in Fig. 7(b). Moreover, for Lena image which is much smooth than Baboon image, *WPSNR* is closer to *PSNR*. This indicates that the quality evaluation criterion of *WPSNR* is closer to the real visual effect for texture images. So the larger strength can be used for watermark embedding in more strong texture image without sacrificing perceptual quality according to the *WPSNR*, just as the watermark strength applied into the Baboon image. When Gaussian noise of the mean value 0 and the variance 0.005 is injected into the watermarked image "Baboon", the *NC* of the extracted watermark image is 0.99, as shown in Fig. 7(d).

We also use JPEG compression to test the robustness of the proposed algorithm. As shown in Fig. 8, when the compression quality factors are larger than 20, the correct recognition rates of watermark logo always stay above 90% for the two test images with different watermark embedding strengths.

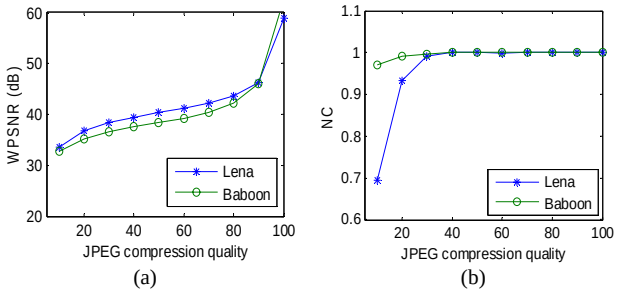

(a) (b)

Figure 8. (a): *WPSNR* of the carrier images corresponding to the different JPEG compression quality factors for "Lena" and "Baboon" (b) *NC* of the extracted watermark Logo corresponding to the different JPEG compression quality factors for "Lena" and "Baboon"

Simultaneously, we test our proposed watermarking algorithm's robustness to different common image processing including 3*3 median filter, Gaussian noise superimposed, wiener filter, etc. Experimental results listed in Tab. 2 show that the *NC* of the extracted watermark logo mostly stays above 0.9. However the robustness of the carrier image "Lena" is poorer than that of "Baboon" with almost the same visual quality *WPSNR* because of the lower embedding strength. It indicates that better robustness performance can be obtained for the images with more complex texture.

TABLE II.
ROBUSTNESS TEST RESULTS OF THE PROPOSED ALGORITHM

Image processing	Lena			Baboon		
	PSNR	WPSNR	NC	PSNR	WPSNR	NC
salt and pepper noise with noise density 0.005	27.7	30.3	0.94	27.5	35.1	1.00
20% JPEG compression	34.1	36.7	0.93	27.5	35.2	0.99
3×3 median filter	38.2	40.8	0.97	27.6	35.2	0.97
wiener filter	36.5	39.1	0.78	27.9	35.6	0.94
Gaussian low-pass filter	45.3	47.9	1.00	36.1	43.8	1.00
1/4 cropping	10.9	13.5	0.86	10.4	18.0	0.86

V. CONCLUSIONS

Considering the intrinsic "wrap around" effect of FRAT, this paper gives a novel blind watermarking algorithm based on the statistical study of energy distributions in the FRIT domain. After orthonormal FRIT transform of the pieces of an image, the classification is carried out twice to get image regions with different texture characteristics by FCM. The first classification is to selected pieces with the strong edges and complex texture for watermark embedding. The second classification is to determine the watermark embedding strength corresponding to the texture pieces with different texture activity degree. For better descriptions of the image texture in ridgelet domain, the total variation of each direction in the FRIT domain and the total energy of the energy dispersion directions used to make up for the 'wrap around' effect for FRIT are considered into FCM, which are nonlinearly processed based on the characteristic of HVS before classifying these pieces. The watermark is embedded into the middle ridgelet subband coefficients of the most significant directions of the selected texture pieces with different embedding strengths, which are determined by experiments based on the improved measures *WPSNR*. And the watermark logo can be extracted without the original image. Experiment results show that the proposed watermark image get good the transparency and robustness. But due to the complexity of the human visual system and the complexity distributions of the oscillating ridgelet coefficients caused by the "wrap around" effect, the proposed watermarking system still have limitation for application, such as the determination of the texture activity degree by the statistical analysis method, which should be solved in future. In addition, the next work also includes adaptively determinations of the watermark embedding strengths based on the texture characteristics of the carrier image and HVS.

ACKNOWLEDGMENT

This work is supported by young and middle-aged foundation of Xi'an Institute of Post and Telecommunications (110-0420).

REFERENCES

[1] A. Briassouli, P. Tsakalides, and A. Stouraitis, "Hidden messages in heavy-tails: DCT-domain watermark detection using alpha-state model", *IEEE Transactions on Multimedia*, vol. 7, no. 4, 2005, pp. 700-714.

[2] J. X. Zhang, J. W. Zhang, and J. Z. Sun. "Image-adaptive and robust digital wavelet-domain watermarking for image", *Journal of Communication and Computer*, vol.2, 2005, pp. 57-63.

[3] E. Candes and D. L. Donoho. "Ridgelets: a key to higher-dimensional intermittency?", *Phil. Trans. R.* Soc. Lond. A. 1999, pp. 2495–2509.

[4] M. N. Do and M. Vetterli. "Orthonormal finite ridgelet transform for image compression", *IEEE Image Processing*, vol. 2, 2000, pp. 367-370.

[5] M. N. Do and M. Vetterli . "The Finite Ridgelet Transform for Image Representation", *IEEE Image Processing*,, vol. 12, no. 1, 2003, pp. 16-28.

[6] Y. X. Liu, Y. H. Peng, H. J. Qu, and Y. Yin, "Energy-based adaptive orthogonal FRIT and its application in image denoising", *Science in China Series E-Information Science*, vol. 37, no. 4, 2007, pp. 514-526.

[7] Z. H. Xie, S. Q. Wang, L. X. Gan, L. Zhang, and Z. H. Shu, "Content based image watermarking in the ridgelet domain", *International Symposium Electronic Commence and Security*, vol. 32, 2008, pp. 877-800.

[8] N. R. Pal and J. C. Bezdek, "On cluster validity for the fuzzy C-means Model", *IEEE Transactions on Fuzzy System*, vol. 3, no.3, 1995, pp. 370-379.

[9] D. L. Donoho. "Fast ridgelet transforms in dimension 2". *Technical* report, Stanford University, Department of Statistics, Stanford CA 94305–4065, 1997

[10] L. Xiao, Z. H. Wei, and H. Z. Wu, "Embedding Image Watermarks into Local Linear Singularity Coefficients in Ridgelet Domain", *VSMM2006, LNCS4270*, 2006, pp. 119-127.

[11] L. Xiao, Z. H. Wei, and H. Z. Wu, "Image adaptive watermarking algorithm based on noise visible control in ridgelet domain", *Chinese Journal of Scientific Instrument*, vol. 29, no. 1, 2008, pp. 167-173.

[12] C.-T. Hsu and J.-L. Wu, "Hidden signatures in images," *Proc. IEEE Int. Conf. Image Procesing*, vol. 3, Lausanne, Switzerland, pp. 223–226, Sep. 1996.

[13] S. Voloshynovskiy, A. Harrigel, N. Baumgartner, and T. Pun, "A stochastic approach to content adaptive digital image watermarking," *Proc. Int. Workshop on Information Hiding, LNCS*, vol. 1768, pp. 211-236, Sep. 1999.

Hai-yan Yu: female, born in 1982, master, and instructor. She received Master Degree form Xi'an University of Technology in 2006. Since 2006 she has served as a teacher at Xi'an Institute of Post and Telecommunications. Her research interests include wavelet algorithm, fuzzy information and image processing.

Jiu-lun Fan: male, born in 1964, professor, and advisor for doctoral students. He received his Ph.D in signal and information processing from the Xidian University in 1998. He is the chairman of the department of information and control in Xi'an Institute of Post and Telecommunications. He has long been engaged in the teaching and research in the field of fuzzy information processing. He has successively undertaken or taken charge of many key projects. His research interests focus on pattern recognition, fuzzy system and image processing.